Am J Transl Res 2026;18(3):1959-1971
www.ajtr.org /ISSN:1943-8141/AJTR0169358

Original Article

Hyperoside promotes osteoblast differentiation by increasing osteoclast-derived migrasomes to alleviate osteoporosis

Shu Yan[1], Zhenguo Luo[1], Bingqin Ma[1], Jiajia Dou[2], Lvmei Liu[1], Lujie Miao[3]

[1]Department of General Practice, The Third Affiliated Hospital of Soochow University, Changzhou 213003, Jiangsu, China; [2]Soochow University, Suzhou 215000, Jiangsu, China; [3]Department of Gastroenterology, The Third Affiliated Hospital of Soochow University, Changzhou 213003, Jiangsu, China

Received October 16, 2025; Accepted January 30, 2026; Epub March 15, 2026; Published March 30, 2026

Abstract: Objectives: Osteoporosis, resulting from an imbalance between osteoblast-mediated bone formation and osteoclast-mediated bone resorption, can be alleviated by hyperoside. Migrasomes, as newly discovered extracellular vesicles, play a crucial role in mediating intercellular communication. However, it remains unclear whether hyperoside alleviates osteoporosis by mediating intercellular communication between osteoblasts and osteoclasts through migrasomes. This study investigates the potential therapeutic mechanisms of hyperoside in treating osteoporosis using an ovariectomized mouse model. Methods: Hyperoside was administered to the mice by intragastric gavage daily for 2 months. Micro-CT scans and histopathological analyses were performed to evaluate bone formation. Migrasomes derived from hyperoside-treated osteoclasts were characterized by transmission electron microscopy, Western blot, and immunofluorescence, and subsequently used to treat osteoblasts followed by RNA sequencing. Results: Micro-CT scans and histopathological evaluations showed that hyperoside reduced bone resorption and osteoclast numbers in ovariectomized mice. Immunofluorescence staining revealed that hyperoside increased the expression of osteoblast regulators OPG and RUNX2. Hyperoside increased migrasome secretion from osteoclasts, which was validated by transmission electron microscopy and Western blot analyses. Migrasomes were then used to treat MC3T3-E1 cells, boosting osteoblast marker expressions and differentiation. RNA sequencing of migrasomes showed distinct regulatory patterns, with upregulated genes in the hyperoside-treated migrasomes compared to the control linked to immune responses, iron ion homeostasis, oxidative stress, and apoptosis, and downregulated genes related to lipid metabolism. Notably, hyperoside-regulated migrasomes also affected ferroptosis by increasing ferroptosis repressors Nr4a1, Lcn2, Nupr1, and Zfp36. Conclusions: These findings suggest that hyperoside exerts its osteogenic effects through migrasome-mediated crosstalk, offering new insights into the treatment of osteoporosis.

Keywords: Osteoporosis, osteoblast, hyperoside, migrasomes, ferroptosis

Introduction

Osteoporosis is a highly prevalent metabolic bone disease that increases bone fragility and the risk of fractures, and it is estimated to affect over 300 million people by 2040 [1]. The disease arises from an imbalance between bone-resorbing osteoclasts and bone-forming osteoblasts, in which excessive osteoclast activity and reduced osteoblast function lead to bone loss and deterioration of bone microarchitecture [2]. This process can be further accelerated by aging, hormonal changes, environmental influences, or unhealthy lifestyles, such as insufficient calcium intake and lack of exercise [3, 4]. Bone remodeling relies on the coordinated actions of osteoclasts and osteoblasts involving intercellular contact, extracellular matrix interactions, and cytokine release [5]. Disruption in their communication may contribute to bone disorders [6]. Osteoblast-derived extracellular vesicles can shift activity from bone formation to resorption [7], while vesicles aid bone repair via the TGFβ1/SMAD3 pathway [8]. The interaction between these cells affects osteogenesis. For example, osteoclastogenesis is inhibited when osteoclasts are co-cultured with ED-71-treated osteoblasts, improving bone

https://doi.org/10.62347/GNGB6008

mass in ovariectomized (OVX) rats [9]. BMP2 immune complexes promote bone formation by facilitating direct interactions between osteoclasts and osteoblasts [10]. Thus, drugs targeting these interactions could help prevent and treat osteoporosis.

Hyperoside, a key bioactive compound in *Hypericum* species [11], exhibits significant pharmacological activities, including anti-cancer, antibacterial, antiviral, and neuroprotective effects [12-14]. Recent research highlights its potential in treating postmenopausal osteoporosis by inhibiting bone resorption through the miR-19a-5p/IL-17A axis [15] and the ERα/ITGβ3 signaling pathway [16]. It also affects the TRAF6-dependent RANKL/RANK/NF-κB signaling and increases the OPG/RANKL ratio [17]. While studies have explored its role in reducing osteoclast activity and promoting osteoblast function, the interaction between these cells in achieving its osteoprotective effects remains unexplored.

Migrasomes are newly discovered extracellular vesicles that are formed in migrating cells and mediate intercellular communication [18]. Migrasomes originate from membrane tubule structures (approximately 50-300 nm in diameter) left behind by migrating cells and remain connected to the parent cell via retraction fibers before eventually detaching and being released [19]. Migrasomes are enriched with diverse signaling molecules, including cytokines, chemokines, and growth factors. These bioactive components can be internalized by neighboring cells, subsequently modulating the behavior and phenotypic states of the recipient cells [20]. The filopodia and migrasome-like vesicles were observed during the migration of osteoclasts, which was described to participate in the spatiotemporal coupling process between osteoclast and osteoblast [21]. Observed migrasomes during osteoclast migration may be involved in osteoclast-osteoblast interactions, though their role in bone remodeling and communication is not well understood. The impact of hyperoside on migrasomes and their function in bone processes also remains unclear.

This study explored the therapeutic effects of hyperoside on osteoporosis in an OVX mouse model. We isolated and characterized hyperoside-induced osteoclast migrasomes and evaluated their role in regulating osteoblast differentiation. RNA sequencing profiling of hyperoside-induced migrasomes enhanced our understanding of their genetic regulation in osteogenic differentiation. Our findings highlight the substantial efforts of migrasomes in the anti-osteoporosis effect of hyperoside and provide novel insights into the prevention and treatment of osteoporosis.

Materials and methods

Animals

Female C57BL/6J mice (8-week-old, n = 18) from Beijing SiPeiFu were housed under controlled conditions (temperature 24-26°C, humidity 55-60%, 12 h light/dark cycle) with free access to water and were randomly divided into sham, OVX, and OVX + Hyperoside groups (6 mice/group). The mice were anesthetized by intraperitoneal injection of 1% Avertin (0.2 mL/10 g, M2910, Nanjing Aibei). Mice in the OVX and OVX + Hyperoside groups underwent ligation of the oviducts and removal of both ovaries, while the mice in the sham group underwent laparotomy only. One week later, the mice in the OVX + Hyperoside group received a daily gavage of hyperoside (40 mg/kg, 482-36-0, Plant Original Biological) for two months [15], whereas the mice in the sham and OVX groups were administered 0.9% saline daily via gavage for two months. After the experimental period, the mice were euthanized by CO_2 inhalation, and their left femurs were collected for subsequent studies. The research followed protocols approved by the Animal Ethics Committee of Yosu (approval number YS-m202506003) and met the guidelines of their responsible governmental agency.

Micro-CT

Micro-CT analysis of femurs was performed on harvested femurs using a Hiscan XM Micro CT (Szhiscan, Suzhou). Three-dimensional reconstructions were performed with Hiscan Reconstruct software (Szhiscan, Suzhou). The bone microstructure measurements were obtained from 3D analysis of the selected bone using Hiscan Analyzer software (Szhiscan, Suzhou). Bone microstructure measurements, including the bone volume fraction (BV/TV), bone surface density (BS/TV), trabecular separation (Tb.Sp), and trabecular number (Tb.N), were obtained using Hiscan Analyzer software.

Cell culture

RAW 264.7 cells (iCell-m047, iCell) were maintained in DMEM (10-013-CVRC, CORNING) containing 10% fetal bovine serum (10099-141C, GIBCO) and 1% penicillin/streptomycin (E607011, Sangon). To induce osteoclast differentiation, RAW 264.7 cells were plated in 24-well plates at a cdensity of 2 × 105 cells/mL and exposed to 50 ng/mL lipopolysaccharide (LPS, L8880, Solabao) for 7 days. Hyperoside (50 μM) was used to treat osteoclasts for 24 h, followed by the extraction of migrasomes.

MC3T3-E1 cells (CL-0378, Procell) were seeded on gelatin-coated six-well plates and incubated in a basal medium for MC3T3-E1 subclone 14 cells osteogenic differentiation (PD-033, Procell) to promote differentiation into osteoblasts. After the formation of osteogenic cells, the cells were incubated with 100 μg of migrasomes for 24 h.

The experiment involved cells that were confirmed to be mycoplasma-free, with PCR testing for any mycoplasma contamination.

Hematoxylin and Eosin (H&E) staining

Femur samples were subjected to decalcification in an EDTA solution, followed by dehydration in graded ethanol, clearing in xylene, and embedding in paraffin. Serial cross-sections (4 μm thickness) were obtained using a microtome and mounted on slides for H&E staining. Histological examination was performed under a light microscope (CK31, Olympus) for morphological analysis.

Tartrate-resistant acid phosphatase (TRAP) staining

Paraffin-embedded sections were deparaffinized with glycol ether acetate and rehydrated through a graded ethanol series. After marking the tissue sections with a histology pen, they were incubated in a humidified chamber with distilled water at 37°C for 2 h. The sections were then incubated in TRAP staining solution at 37°C for 20 min following the removal of the distilled water. The staining solution was then decanted, and the sections were rinsed with water before counterstaining the nuclei with hematoxylin for 15 seconds. Image analysis was conducted using a microscope (Nikon Eclipse E100, Nikon).

Cells were processed according to the manufacturer's protocol (G1492, Solarbio), starting with fixation in TRAP-specific fixative at 4°C for 1 min, followed by incubation with TRAP staining solution at 37°C for 60 min under humidified conditions. After thorough washing, the samples were counterstained with hematoxylin for 5 min to enhance nuclear visualization. The stained specimens were then examined and digitally captured using an Olympus CK31 light microscope equipped with high-resolution imaging capabilities for detailed morphological analysis.

Immunofluorescence

After standard processing, paraffin-embedded tissue sections and cultured cells were prepared sequentially, starting with fixation in 4% paraformaldehyde for 15 min at room temperature. They were permeabilized with 0.3% Triton X-100 in PBS for 10 min, and then blocked with 3% BSA in PBS for 1 h. Next, the samples were incubated overnight at 4°C with the specified primary antibodies: anti-OPG (83065-2-RR, Proteintech), anti-RUNX2 (20700-1-AP, Proteintech), anti-Tspan4 (PA569344, Thermo Fisher Scientific), and anti-TRAP (67315-1-Ig, Proteintech). After washing, appropriate fluorescent-conjugated secondary antibodies (A05-21, Beyotime) were applied for 1 h at room temperature. Nuclei were counterstained with DAPI (1 μg/mL) for 5 min, and fluorescent signals were captured using a Nikon Eclipse Ti inverted fluorescence microscope.

Migrasome isolation

Cells and migrasomes were trypsinized and collected in a 50 mL conical tube, with all steps done at 4°C. The suspension was sequentially centrifuged at 1,000× g for 10 min and 4,000× g for 20 min to remove cells and debris. The supernatant was then centrifuged at 20,000× g for 30 min to pellet crude migrasomes, which were washed with PBS and centrifuged again at 20,000× g for 30 min. Migrasomes were further purified using density gradient centrifugation with Optiprep (Sigma-Aldrich, D1556) as the density medium. A discontinuous gradient was prepared by layering the following solutions in sequence (500 μL each): 30% Optiprep, 25% Optiprep, crude migrasome suspension (in 19% Optiprep), 15% Optiprep, 12% Optiprep, 10% Optiprep, 8% Optiprep, 5% Optiprep, and 2% Optiprep.

The cell pellet was resuspended in 137.5 μL of dilution buffer to prepare the crude migrasome fraction. Then, 400 μL of 1× extraction buffer and 252.5 μL of 60% OptiPrep were added to reach an 18% OptiPrep concentration. The mixture was ultracentrifuged at 150,000× g for 4 h at 4°C. Twelve 480 μL fractions were collected from the gradient, diluted with PBS, and centrifuged at 20,000× g for 30 min at 4°C to pellet migrasomes. The pellets were washed twice with PBS to remove contaminants. Fractions with optimal migrasome enrichment, identified by light scattering, were chosen for transmission electron microscopy analysis.

Transmission electron microscope

A 5-10 μL drop of the resuspended solution was placed on the copper grid, allowing it to settle for 1 min. The filter paper was used to absorb the excess liquid from the edge. After rinsing with PBS, 10 μL of phosphotungstic acid was dropped onto the copper grid, letting it settle for 1 min before absorbing the excess liquid with filter paper. The samples were air-dried at room temperature for 2 min before imaging (JEM-1200EX, JEOL).

Alkaline phosphatase (ALP) and Alizarin red staining

The osteoblasts were fixed with 4% paraformaldehyde and stained with the BCIP/NBT Alkaline Phosphatase Color Development Kit (C3206, Beyotime) and Alizarin Red S (PD-033, Procell) after 21 days of migrasome incubation.

RT-qPCR

Total RNA was extracted using Trizol reagent (Sigma) and assessed with a TGem spectrophotometer (TIANGEN, Beijing). RNA integrity was checked via agarose gel electrophoresis before reverse transcription into cDNA with a Thermo kit (K1622). The cDNA was then analyzed by RT-qPCR using Roche's 2× Master Mix Kit (04913914001), with specific primers listed in Table S1.

Western blot

Cell pellets were collected and processed for protein isolation. Proteins were separated and transferred to PVDF membranes, blocked with 5% skimmed milk, and incubated overnight at 4°C with primary antibodies. After that, the membranes were incubated with horseradish peroxidase-conjugated secondary antibodies. The primary antibodies included anti-GAPDH (60004-1-Lg, Proteintech), anti-PIGK (15151-1-AP, Proteintech), anti-CPQ (16601-1-AP, Proteintech), anti-TSPAN4 (PA5-69344, Thermo Fisher Scientific), anti-ALP (18507-1-AP, Proteintech), anti-RUNX2 (20700-1-AP, Proteintech), anti-OCN (16601-1-AP, 20277-1-AP), and anti-OPG (83065-2-RR, Proteintech). Secondary antibodies included goat anti-mouse IgG H&L (RGAM001, Proteintech) and goat anti-rabbit IgG H&L (RGAR001, Proteintech). The protein bands were detected using ChemiScope 6000 (Clinx, Shanghai), and band densities were quantified with ImageJ, normalized to an internal reference, and expressed as a fold change relative to the control.

RNA sequencing

Briefly, total RNA was extracted from migrasomes derived from hyperoside-treated and control osteoclasts (n = 3 per group) using TRIzol reagent (T9424, Sigma). RNA was assessed using a TGem spectrophotometer (TIANGEN, Beijing, China), and RNA integrity was evaluated by agarose gel electrophoresis. High-quality RNA samples were used to create sequencing libraries with the mRNA-seq Lib Prep Kit for Illumina (RK20302, ABclonal). After assessing library quality, sequencing was conducted on the Illumina NovaSeq platform (Mivectorbio, Shanghai, China) to generate paired-end reads. The raw data underwent quality control, adapter trimming, and read filtering to remove low-quality sequences before being mapped to the mouse reference genome. Differentially expressed genes (DEGs) were identified using the DESeq2 package in R, with thresholds of $P < 0.05$ and $|\text{fold change}| > 1$. These DEGs were subsequently subjected to Gene Ontology (GO) and Kyoto Encyclopedia of Genes and Genomes enrichment analyses to explore their functional implications.

Statistical analysis

Statistical data are displayed as the mean ± standard deviation, with error bars included. Each experiment was independently repeated at least three times. Statistical significance between two groups was evaluated using Student's t-test, while one-way ANOVA with Tukey's

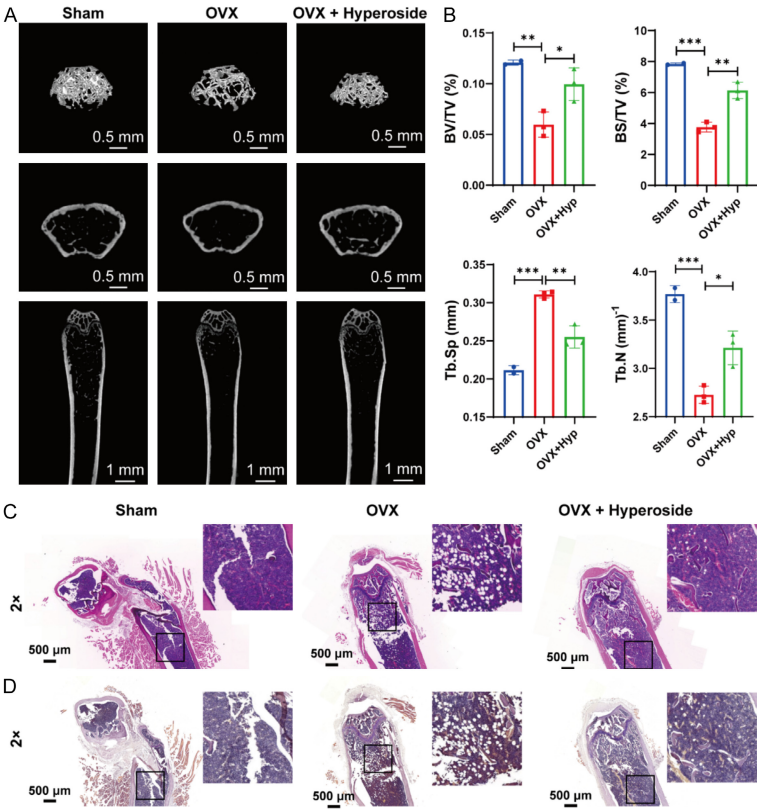

Figure 1. Hyperoside improves osteoporosis in ovariectomized mice. A. Bone composition was assessed by micro-CT scan imaging of the distal femurs. B. The bone microstructure parameters were measured, including bone volume fraction, bone surface density, trabecular separation, and trabecular number. C. Histopathological evaluation of femoral tissues was performed using Hematoxylin and Eosin staining. D. Histopathological evaluation of femoral tissues was performed using tartrate-resistant acid phosphatase (TRAP) staining. One-way ANOVA was used to evaluate statistical significance. *P < 0.05, **P < 0.01, ***P < 0.001, and ****P < 0.0001.

multiple comparisons test was used for comparisons among more than two groups. P < 0.05 was considered statistically significant.

Results

Hyperoside improves osteoporosis in OVX mice

To investigate the therapeutic effects of hyperoside on osteoporosis, a postmenopausal osteoporosis mouse model was established via OVX. The OVX + Hyperoside group received a daily oral dose of 40 mg/kg hyperoside for 2 months. At the end of the treatment, we assessed bone composition by micro-CT scan imaging of the distal femurs (**Figure 1A**). The micro-CT analysis demonstrated that hyperoside mitigated bone resorption in OVX mice (**Figure 1A**). OVX significantly decreased BV/TV, BS/TV, and Tb.N of mice and increased Tb.Sp (**Figure 1B**). Conversely, hyperoside treatment reversed these changes (**Figure 1B**), as confirmed by histopathological evaluation of femoral tissues (**Figure 1C** and **1D**). Specifically, H&E staining revealed significant histological changes caused by OVX in bone sections, such as increased spacing, decreased thickness, and trabecular bone number (**Figure 1C**). Hyperoside treatment effectively reversed OVX-induced bone deterioration (**Figure 1B**). TRAP staining demonstrated a significant increase in TRAP-positive osteoclasts in OVX mice relative to sham controls (**Figure 1D**). In contrast, hyperoside administration mitigated this OVX-induced elevation in osteoclast (**Figure 1D**). Osteoprotegerin (OPG), produced by osteoblasts, prevents osteoclast formation and bone resorption [22]. Runx2 can facilitate osteogenic differentiation [23]. Immunofluorescence staining revealed that OVX suppressed the expression of both OPG and RUNX2, whereas hyperoside treatment upregulated their expression (**Figure 2A** and **2B**), suggesting that hyperoside-mediated anti-osteoporotic mechanism may involve modulation of osteoclast-mediated bone resorption.

Hyperoside promotes osteoclast-derived migrasome secretion

The interaction between osteoclasts and osteoblasts, as well as their cellular communication, plays a critical role in osteoporosis development [6]. Migrasomes facilitate intercellular communication, but it's unclear if hyperoside affects osteoclast-osteoblast interaction through migrasomes. We aim to explore hyperoside's impact on osteoclast-derived migrasomes and their effect on osteoblast activity. LPS was used to induce RAW264.7 cells differentiation into osteoclasts, as confirmed by

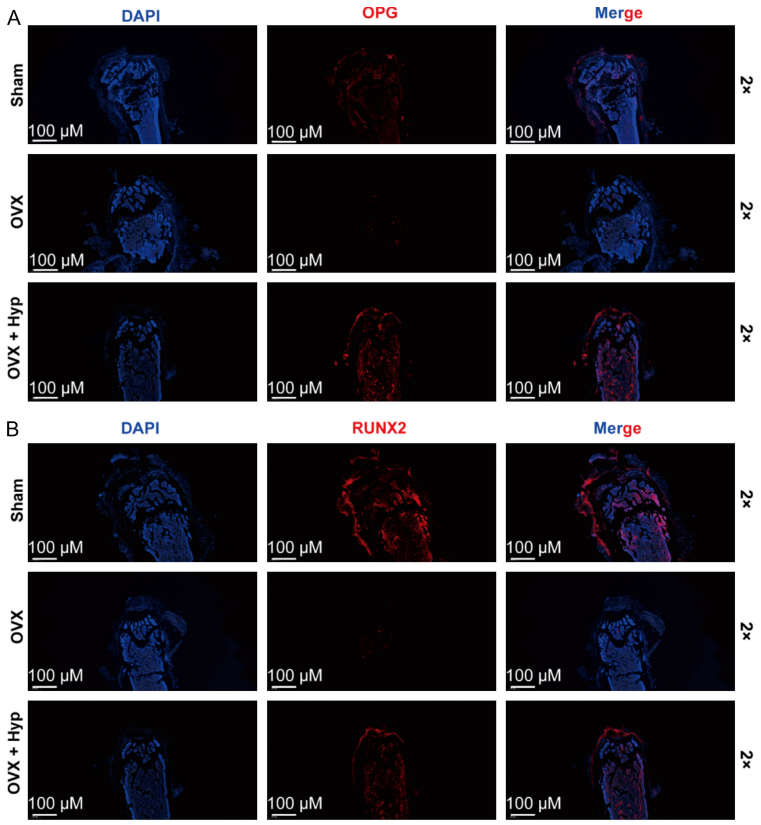

Figure 2. Hyperoside regulates osteoblast markers OPG and RUNX2. A, B. Immunofluorescence staining revealing the levels and localization of OPG (A) and RUNX2 (B) in femurs.

TRAP staining (**Figure 3A**). We isolated migrasomes from hyperoside-treated osteoclasts and confirmed their presence under transmission electron microscope observations (**Figure 3B**). Ultrastructural analysis showed that the vesicles had a pomegranate-like shape and were connected to fibrous filaments (**Figure 3B**). Equal amounts of migrasome proteins from each group were used for Western blot analysis, revealing migrasome-related proteins in the isolated migrasomes, but these proteins were scarcely found in intracellular fractions (**Figure 3C**). Meanwhile, we performed immunofluorescence staining with equal amounts of cells from each group to validate the presence of migrasomes in osteoclasts. We observed co-localization of the migrasome marker TSPAN4 with the osteoclast marker TRAP (**Figure 3D**). Hyperoside increased migrasome secretion per cell while reducing the number of $TRAP^+$ osteoclasts (**Figure 3D**), suggesting that hyperoside promotes migrasome generation in osteoclasts.

Hyperoside regulates osteoblast differentiation through migrasomes

To assess if hyperoside influences osteoblast differentiation via migrasomes, we exposed MC3T3-E1 cells to migrasomes from hyperoside-stimulated osteoclasts. RT-qPCR showed that these migrasomes significantly increased mRNA levels of osteoblast markers (Alp, Runx2, Ocn, and Opg) compared to controls (**Figure 4A**). Western blot analysis confirmed higher protein levels of ALP, RUNX2, OCN, and OPG in cells treated with hyperoside-induced migrasomes (**Figure 4B**). Furthermore, we assessed osteoblast differentiation using ALP staining (**Figure 4C**) and Alizarin Red staining (**Figure 4D**). ALP represents the hallmark enzyme of mature osteoblasts and was visualized as granular or patchy gray-brown to dark-black precipitates in the cytoplasm (**Figure 4C**). Alizarin Red staining detected calcium deposition induced by osteoblasts, indicating enhanced osteogenic capacity (**Figure 4D**). We observed more intense ALP and Alizarin Red staining in the hyperoside-treated group compared to the control group (**Figure 4C** and **4D**). This suggests that hyperoside enhances osteoblast differentiation and osteogenic capacity, potentially through migrasome-mediated regulation.

Hyperoside-regulated migrasomes mediate ferroptosis

Studies indicate that migrasomes can transfer mRNA and facilitate its expression in recipient cells [24, 25]. To understand how hyperoside improves osteoporosis via migrasomes, we conducted RNA sequencing on migrasomes from hyperoside-treated and control osteoclasts. Transcriptional profiling revealed distinct regulatory patterns in hyperoside-treated migrasomes compared to controls (**Figure 5A**). Comparative analysis identified 839 DEGs between the hyperoside and control groups,

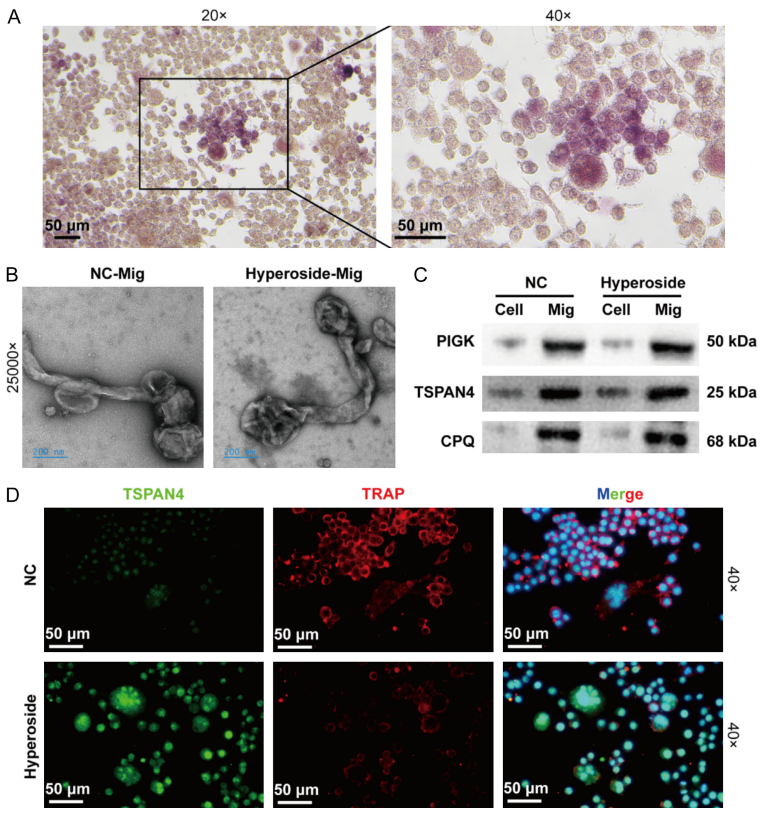

Figure 3. Hyperoside regulates the generation of migrasomes derived from osteoclasts. A. Tartrate-resistant acid phosphatase staining revealed that RAW264.7 cells were induced by lipopolysaccharide to differentiate into osteoclasts. B. Transmission electron microscope analysis of migrasomes isolated from hyperoside-treated osteoclasts. C. Western blot analysis demonstrated the levels of migrasome-related proteins in the cells and the isolated migrasomes. D. Immunofluorescence staining depicting the co-localization of the migrasome marker TSPAN4 with the osteoclast marker TRAP.

including 376 upregulated and 463 downregulated DEGs in the hyperoside compared to the control (**Figure 5B**). Notably, upregulated DEGs were associated with immune responses (e.g. cytokine-cytokine receptor interaction, NF-kappa B signaling pathway, TNF signaling pathway, and Toll-like receptor signaling pathway), apoptosis, and osteoclast differentiation (**Figure 5C**), while downregulated DEGs were involved in lipid metabolism, such as biosynthesis of unsaturated fatty acids, fatty acid metabolism, arachidonic acid metabolism, and ovarian steroidogenesis (**Figure 5D**). GO enrichment analysis further supported these findings (**Figure 5E**). Dysregulation of iron homeostasis induces oxidative stress that critically drives ferroptosis activation [26, 27]. We noticed that the upregulated DEGs were linked to iron ion homeostasis, while the downregulated DEGs participated in oxidative stress (**Figure 5E**), suggesting that hyperoside-modified migrasomes influence ferroptosis. By intersecting DEGs from RNA sequencing with ferroptosis-related genes from GeneCards (**Figure 6A**), 46 overlapping DEGs were identified, including Nr4a1, Lcn2, Nupr1, and Zfp36, which are associated with osteogenic differentiation [28-31] and act as ferroptosis repressors [32-35]. RT-qPCR revealed that hyperoside significantly upregulated the expression of these four ferroptosis repressors in migrasomes (**Figure 6B**), indicating that hyperoside may enhance osteogenic differentiation by inhibiting migrasomes-mediated ferroptosis.

Discussion

Osteoporosis is a metabolic bone disorder marked by reduced bone mass and deteriorated microarchitecture, with pathogenesis involving complex cellular and molecular mechanisms [36]. Recent studies identify migrasomes, a novel type of extracellular vesicle, as key mediators of intercellular communication [18, 20]. This study explored the therapeutic potential of hyperoside in an OVX mouse model of osteoporosis and elucidated the critical role of migrasomes in this process. Our results demonstrated that hyperoside significantly increased bone mineral density in OVX mice and alleviated osteoporotic symptoms by modulating osteoclast and osteoblast activity. Mechanistically, hyperoside enhanced the production of osteoclast-derived migrasomes, which carried specific signaling molecules likely influencing osteoblast differentiation and function. These findings suggest a new treatment strategy for osteoporosis and support migrasome-based interventions in bone metabolic disorders.

The dynamic balance between osteoclasts and osteoblasts is crucial for maintaining bone metabolic homeostasis. In osteoporosis, enhanced osteoclast activity leads to excessive bone

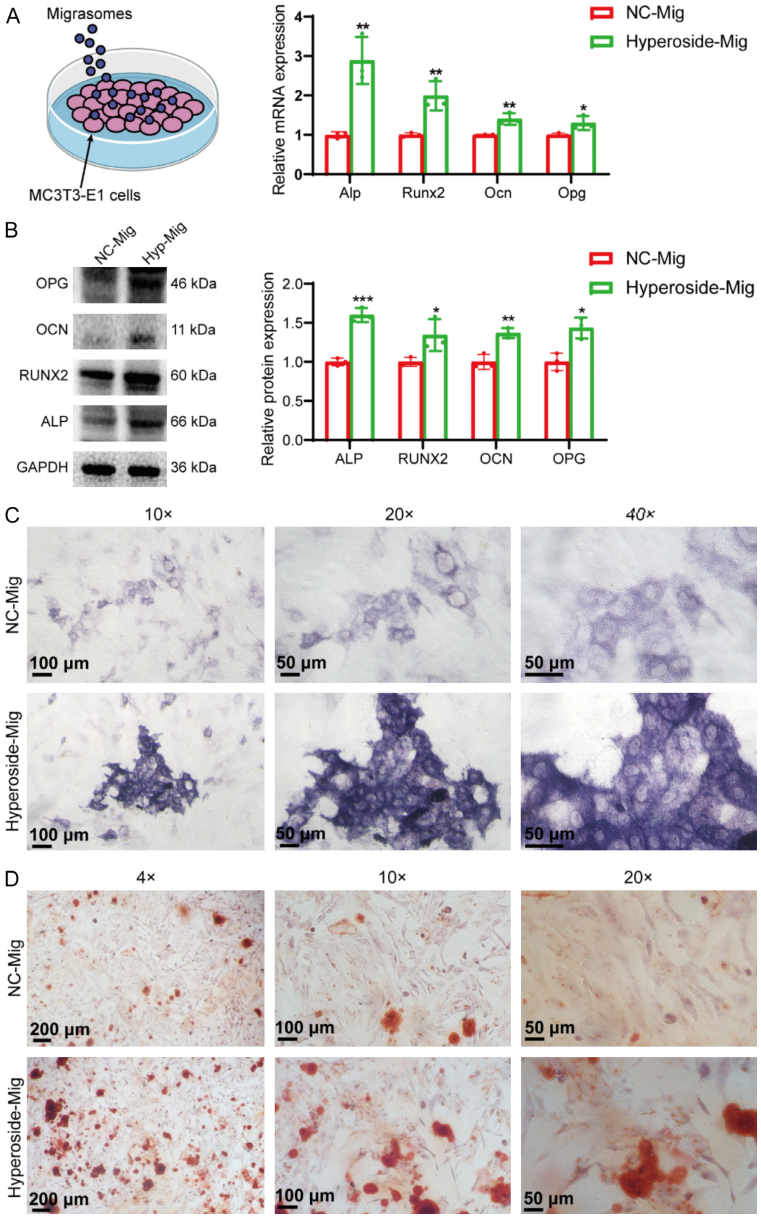

Figure 4. Hyperoside regulates osteoblast differentiation mediated by migrasomes. A. The left panel illustrates the schematic diagram of cell treatment. The right is RT-qPCR analysis, revealing mRNA levels of osteoblast marker genes in hyperoside-induced osteoclast migrasome-treated MC3T3-E1 cells, including Alp, Runx2, Ocn, and Opg. B. Western blot analysis demonstrated the protein levels of ALP, RUNX2, OCN, and OPG in osteoblasts. C. Alkaline phosphatase staining was used to assess osteoblast differentiation. D. Alizarin Red staining detected calcium deposition induced by osteoblasts. Student's t-test was used to evaluate statistical significance between the groups. $*P < 0.05$, $**P < 0.01$, and $***P < 0.001$.

resorption compared to bone formation, resulting in bone loss [37]. Extracellular vesicles serve as a novel mechanism mediating communication between osteoclasts and osteoblasts. For instance, osteoclast-derived exosomes carrying lncRNA AW011738 can be internalized by osteoblasts to inhibit osteoblast function and exacerbate osteoporosis [38], while osteoblast-derived exosomes containing miR-503-3p can prevent osteoclast differentiation [39], highlighting extracellular vesicle-mediated intercellular regulation in bone remodeling. Our in vitro studies demonstrate that hyperoside regulates migrasome production in osteoclasts, which subsequently influences osteoblast differentiation. Specifically, migrasomes isolated from hyperoside-treated osteoclasts significantly upregulated the expression of osteogenic markers (Alp, Runx2, Ocn, and Opg) in osteoblasts, promoting their differentiation and mineralization. In fact, recent work has shown that tumor cell derived migrasomes can promote osteoclast differentiation via direct transfer of cytoplasmic components [40], suggesting that migrasomes indeed play an important role in bone cell crosstalk. Our findings first suggest that migrasomes serve as intercellular messengers transmitting signals from osteoclasts to osteoblasts to regulate bone remodeling.

RNA sequencing of hyperoside-treated migrasomes showed an enrichment of immune-related genes. Bone immunology is crucial for balancing bone remodeling and resorption, essential for skeletal integrity [41, 42]. For instance, LPS increases proinflammatory cytokines and inhibits osteoblast differentiation [43], while inflammation expands osteoclast precursors, leading to bone loss [44]. Intriguingly, hyperoside treatment reduced migrasome-delivered genes linked to inflammatory pathways like NF-kappa B, TNF, and Toll-like receptor signaling pathways. This osteoclast-osteoblast immunoregulatory communication

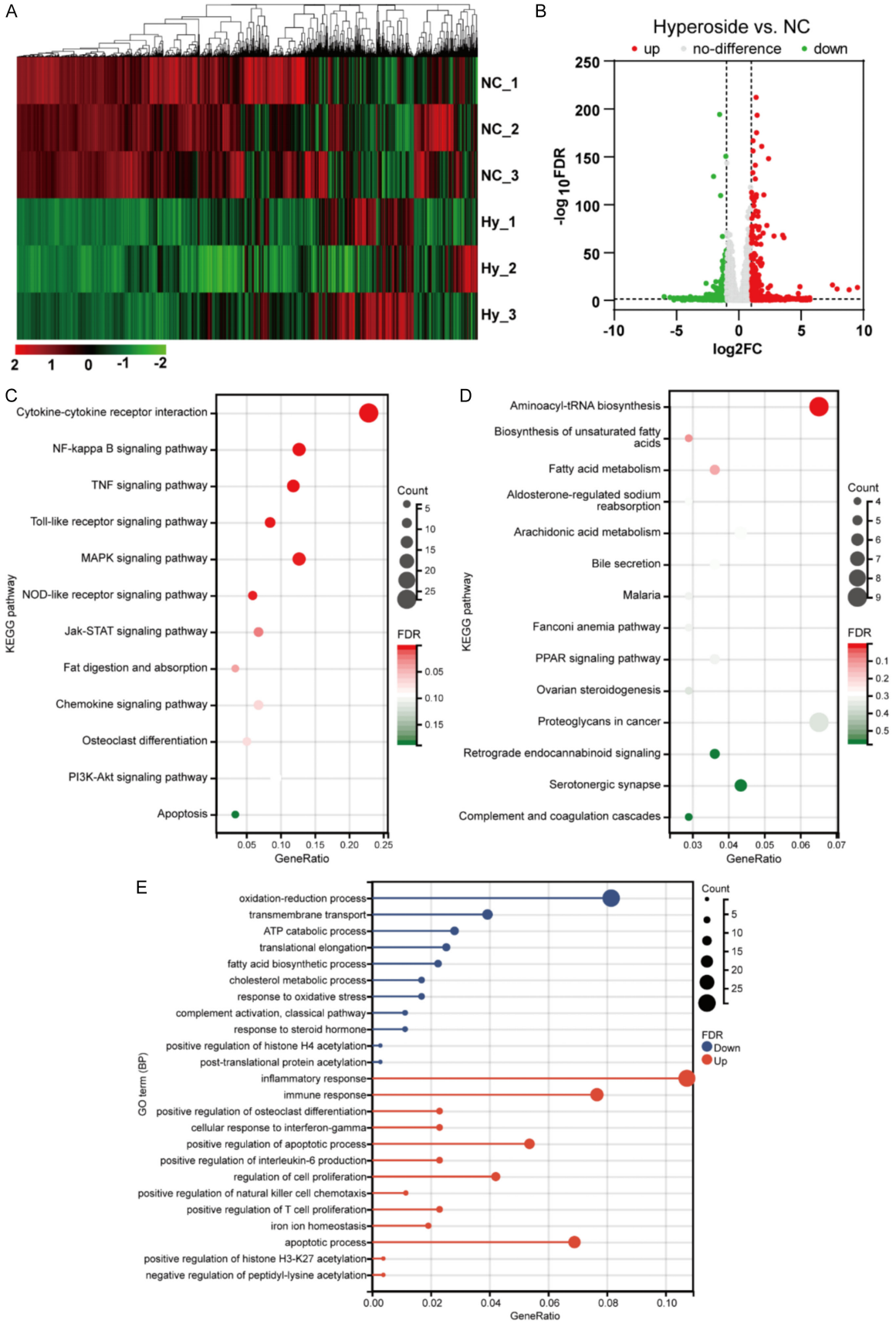
A
NC_1
NC_2
NC_3
Hy_1
Hy_2
Hy_3
2 1 0 -1 -2
B
Hyperoside vs. NC
up
no-difference
down
-log 10FDR
log2FC
C
Cytokine-cytokine receptor interaction
NF-kappa B signaling pathway
TNF signaling pathway
Toll-like receptor signaling pathway
MAPK signaling pathway
NOD-like receptor signaling pathway
Jak-STAT signaling pathway
Fat digestion and absorption
Chemokine signaling pathway
Osteoclast differentiation
PI3K-Akt signaling pathway
Apoptosis
KEGG pathway
GeneRatio
Count
FDR
D
Aminoacyl-tRNA biosynthesis
Biosynthesis of unsaturated fatty acids
Fatty acid metabolism
Aldosterone-regulated sodium reabsorption
Arachidonic acid metabolism
Bile secretion
Malaria
Fanconi anemia pathway
PPAR signaling pathway
Ovarian steroidogenesis
Proteoglycans in cancer
Retrograde endocannabinoid signaling
Serotonergic synapse
Complement and coagulation cascades
KEGG pathway
GeneRatio
Count
FDR
E
oxidation-reduction process
transmembrane transport
ATP catabolic process
translational elongation
fatty acid biosynthetic process
cholesterol metabolic process
response to oxidative stress
complement activation, classical pathway
response to steroid hormone
positive regulation of histone H4 acetylation
post-translational protein acetylation
inflammatory response
immune response
positive regulation of osteoclast differentiation
cellular response to interferon-gamma
positive regulation of apoptotic process
positive regulation of interleukin-6 production
regulation of cell proliferation
positive regulation of natural killer cell chemotaxis
positive regulation of T cell proliferation
iron ion homeostasis
apoptotic process
positive regulation of histone H3-K27 acetylation
negative regulation of peptidyl-lysine acetylation
GO term (BP)
GeneRatio
Count
FDR
Down
Up

Figure 5. Hyperoside-regulated migrasomes mediate ferroptosis. (A) Transcriptional profiling of hyperoside-regulated migrasomes derived from osteoclasts. (B) Volcano plot identified differentially expressed genes (DEGs) between the hyperoside and control groups. (C, D) Kyoto Encyclopedia of Genes and Genomes enrichment analysis of upregulated (C) and downregulated (D) DEGs in the hyperoside group compared to the control group. (E) Gene Ontology enrichment analysis of upregulated and downregulated DEGs in the hyperoside group compared to the control group.

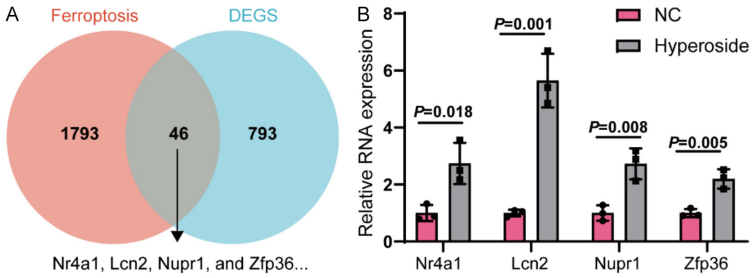

Figure 6. Hyperoside-mediated migrasomes highly express ferroptosis repressors. A. The differentially expressed genes identified from RNA sequencing were intersected with ferroptosis-related genes obtained from the GeneCards database. B. RT-qPCR analysis showing the expression levels of Nr4a1, Lcn2, Nupr1, and Zfp36 in hyperoside-induced osteoclast migrasomes. Student's t-test was used to evaluate statistical significance between the groups.

may significantly contribute to osteoporosis pathogenesis, and hyperoside appears to restore this dysregulated crosstalk by modulating migrasome biogenesis and function. Furthermore, migrasome-mediated intercellular communication may involve additional cell types and signaling pathways.

Ferroptosis, a regulated cell death dependent on iron and characterized by iron accumulation and lipid peroxidation [45], is implicated in several pathological conditions, including osteoporosis [46]. Our RNA sequencing analysis found significant links between DEGs in hyperoside-treated osteoclast migrasomes and ferroptosis-related pathways (e.g., iron ion homeostasis, oxidative stress, fatty acid metabolism, and ovarian steroidogenesis). Notably, activating ferroptosis can worsen osteoporosis [47]. Previous studies report that estrogen withdrawal induces iron accumulation in bone tissue and ferroptosis in bone cells, which stimulates osteoclastogenesis and reduces bone mineral density [48]. In our findings, key ferroptosis repressors (Nr4a1, Lcn2, Nupr1, and Zfp36) were significantly upregulated in hyperoside-treated migrasomes. This upregulation may contribute to inhibiting migrasome-mediated ferroptosis, thereby promoting osteoblast differentiation and bone formation. Although most studies indicate that extracellular vesicles can modulate ferroptosis, whether migrasomes [49, 50], a specific type of extracellular vesicle, can regulate ferroptosis has been scarcely reported. Our findings suggest a novel mechanism by which hyperoside exerts its osteoprotective effects through the inhibition of ferroptosis via migrasome regulation.

This study has several limitations. First, the OVX mouse model and in vitro cell experiments cannot fully replicate the complexity of human bone remodeling and the osteoblast-osteoclast microenvironment, which may limit clinical translation. Second, although RNA sequencing data of migrasome derived from hyperoside-treated osteoclasts revealed ferroptosis-related genes, the functional roles of key molecules such as Nr4a1, Lcn2, Nupr1, and Zfp36 were not directly validated, and ferroptotic activity was not experimentally confirmed. Third, it remains unclear whether hyperoside promotes osteoblast differentiation primarily by increasing migrasome secretion from osteoclasts or by altering the molecular cargo within migrasomes.

Conclusion

This study highlights hyperoside's significant therapeutic effects on osteoporosis in an OVX mouse model. Hyperoside increases osteoclast-derived migrasomes, which influence osteoblast differentiation and function, alleviating osteoporosis. It also boosts ferroptosis repressors in migrasomes, promoting osteoblast activity and bone formation. These findings offer new insights into osteoporosis treatment and suggest a theoretical basis for using migrasomes in bone metabolic disorders.

Acknowledgements

This study was supported by the Major Scientific Research Project of Changzhou Municipal Health Commission (ZD202311).

Disclosure of conflict of interest

None.

Address correspondence to: Lujie Miao, Department of Gastroenterology, The Third Affiliated Hospital of Soochow University, Juqian Street No. 185, Changzhou 213003, Jiangsu, China. E-mail: miaolujie@aliyun.com; Shu Yan, Department of General Practice, The Third Affiliated Hospital of Soochow University, Juqian Street No. 185, Changzhou 213003, Jiangsu, China. E-mail: yanlimlj@163.com

References

[1] Jones AR, Herath M, Ebeling PR, Teede H and Vincent AJ. Models of care for osteoporosis: a systematic scoping review of efficacy and implementation characteristics. EClinicalMedicine 2021; 38: 101022.

[2] Song S, Guo Y, Yang Y and Fu D. Advances in pathogenesis and therapeutic strategies for osteoporosis. Pharmacol Ther 2022; 237: 108168.

[3] Rasul S, Mashayekhi Y, Javaid M, Merie S, Khalaf MA, Ahmed T, Haris M and Mustafa I. Hormonal changes during menopause and their impact on bone health: insights from orthopedic and reproductive medicine. Cureus 2025; 17: e93224.

[4] Jogi MK, Sharma R, Rahman A, Aglawe A and Joshi V. Key determinants of postmenopausal osteoporosis: a mini-review of current insights. Journal of Reproductive Healthcare and Medicine 2024; 5: 12.

[5] Daponte V, Henke K and Drissi H. Current perspectives on the multiple roles of osteoclasts: mechanisms of osteoclast-osteoblast communication and potential clinical implications. Elife 2024; 13: e95083.

[6] Fu YF, Shi SW, Wu JJ, Yuan ZD, Wang LS, Nie H, Zhang ZY, Wu X, Chen YC, Ti HB, Zhang KY, Mao D, Ye JX, Li X and Yuan FL. Osteoclast secretes stage-specific key molecules for modulating osteoclast-osteoblast communication. J Cell Physiol 2025; 240: e31484.

[7] Uenaka M, Yamashita E, Kikuta J, Morimoto A, Ao T, Mizuno H, Furuya M, Hasegawa T, Tsukazaki H, Sudo T, Nishikawa K, Okuzaki D, Motooka D, Kosaka N, Sugihara F, Boettger T, Braun T, Ochiya T and Ishii M. Osteoblast-derived vesicles induce a switch from bone-formation to bone-resorption in vivo. Nat Commun 2022; 13: 1066.

[8] Faqeer A, Wang M, Alam G, Padhiar AA, Zheng D, Luo Z, Zhao IS, Zhou G, van den Beucken JJJP, Wang H and Zhang Y. Cleaved SPP1-rich extracellular vesicles from osteoclasts promote bone regeneration via TGFbeta1/SMAD3 signaling. Biomaterials 2023; 303: 122367.

[9] Wang K, Kou Y, Rong X, Wei L, Li J, Liu H, Li M and Song H. ED-71 improves bone mass in ovariectomized rats by inhibiting osteoclastogenesis through EphrinB2-EphB4-RANKL/OPG axis. Drug Des Devel Ther 2024; 18: 1515-1528.

[10] Xu Y, Yang Y, Hua Z, Li S, Yang Z, Liu Q, Fu G, Ji P and Wu Q. BMP2 immune complexes promote new bone formation by facilitating the direct contact between osteoclasts and osteoblasts. Biomaterials 2021; 275: 120890.

[11] Wu JJ, Zhang J, Xia CY, Ding K, Li XX, Pan XG, Xu JK, He J and Zhang WK. Hypericin: a natural anthraquinone as promising therapeutic agent. Phytomedicine 2023; 111: 154654.

[12] Choudhary N, Collignon TE, Tewari D and Bishayee A. Hypericin and its anticancer effects: from mechanism of action to potential therapeutic application. Phytomedicine 2022; 105: 154356.

[13] Wang X, Wang L, Fekrazad R, Zhang L, Jiang X, He G and Wen X. Polyphenolic natural products as photosensitizers for antimicrobial photodynamic therapy: recent advances and future prospects. Front Immunol 2023; 14: 1275859.

[14] Farasati Far B, Gouranmohit G, Naimi-Jamal MR, Neysani E, El-Nashar HAS, El-Shazly M and Khoshnevisan K. The potential role of Hypericum perforatum in wound healing: a literature review on the phytochemicals, pharmacological approaches, and mechanistic perspectives. Phytother Res 2024; 38: 3271-3295.

[15] An H, Chu C, Zhang Z, Zhang Y, Wei R, Wang B, Xu K, Li L, Liu Y, Li G and Li X. Hyperoside alleviates postmenopausal osteoporosis via regulating miR-19a-5p/IL-17A axis. Am J Reprod Immunol 2023; 90: e13709.

[16] Wei Q, Ouyang M, Guo X, Fu X, Liu T, Luo Y, Tang H, Yang Y, Gao X and Mao H. Effect of hyperoside on osteoporosis in ovariectomized mice through estrogen receptor alpha/ITGbeta3 signaling pathway. Eur J Pharmacol 2024; 977: 176666.

[17] Chen Y, Dai F, He Y, Chen Q, Xia Q, Cheng G, Lu Y and Zhang Q. Beneficial effects of hyperoside on bone metabolism in ovariectomized mice. Biomed Pharmacother 2018; 107: 1175-1182.

[18] Jiang Y, Liu X, Ye J, Ma Y, Mao J, Feng D and Wang X. Migrasomes, a new mode of intercellular communication. Cell Commun Signal 2023; 21: 105.

[19] Jiang D, Li Y and Yu L. Detection, purification, characterization, and manipulation of migrasomes. Curr Protoc 2023; 3: e856.

[20] Jiao H and Yu L. Migrasomes: biogenesis, physiological roles, and therapeutic potentials. J Cell Biol 2024; 223: e202403051.

[21] Lampiasi N, Russo R, Kireev I, Strelkova O, Zhironkina O and Zito F. Osteoclasts differentiation from murine RAW 264.7 cells stimulated by RANKL: timing and behavior. Biology (Basel) 2021; 10: 117.
[22] Udagawa N, Koide M, Nakamura M, Nakamichi Y, Yamashita T, Uehara S, Kobayashi Y, Furuya Y, Yasuda H, Fukuda C and Tsuda E. Osteoclast differentiation by RANKL and OPG signaling pathways. J Bone Miner Metab 2021; 39: 19-26.
[23] Yang JX, Xie P, Li YS, Wen T and Yang XC. Osteoclast-derived miR-23a-5p-containing exosomes inhibit osteogenic differentiation by regulating Runx2. Cell Signal 2020; 70: 109504.
[24] Zhu M, Zou Q, Huang R, Li Y, Xing X, Fang J, Ma L, Li L, Yang X and Yu L. Lateral transfer of mRNA and protein by migrasomes modifies the recipient cells. Cell Res 2021; 31: 237-240.
[25] Zhang Y, Guo W, Bi M, Liu W, Zhou L, Liu H, Yan F, Guan L, Zhang J and Xu J. Migrasomes: from biogenesis, release, uptake, rupture to homeostasis and diseases. Oxid Med Cell Longev 2022; 2022: 4525778.
[26] Jing X, Wang W, He X, Liu X, Yang X, Su C, Shao Y, Ge Z, Wang H and Cui X. HIF-2alpha/TFR1 mediated iron homeostasis disruption aggravates cartilage endplate degeneration through ferroptotic damage and mtDNA release: a new mechanism of intervertebral disc degeneration. J Orthop Translat 2024; 46: 65-78.
[27] Yang X, Gu C, Cai J, Li F, He X, Luo L, Xiao W, Hu B, Hu J, Qian H, Ren S, Zhang L, Zhu X, Yang L, Yang J, Yang Z, Zheng Y, Huang X and Wang Z. Excessive SOX8 reprograms energy and iron metabolism to prime hepatocellular carcinoma for ferroptosis. Redox Biol 2024; 69: 103002.
[28] Yang K, Wang X, Zhang C, Liu D and Tao L. Metformin improves HPRT1-targeted purine metabolism and repairs NR4A1-mediated autophagic flux by modulating Fox01 nucleocytoplasmic shuttling to treat postmenopausal osteoporosis. Cell Death Dis 2024; 15: 795.
[29] Xia Y, Ge G, Xiao H, Wu M, Wang T, Gu C, Yang H and Geng D. REPIN1 regulates iron metabolism and osteoblast apoptosis in osteoporosis. Cell Death Dis 2023; 14: 631.
[30] Murayama M, Hirata H, Shiraki M, Iovanna JL, Yamaza T, Kukita T, Komori T, Moriishi T, Ueno M, Morimoto T, Mawatari M and Kukita A. Nupr1 deficiency downregulates HtrA1, enhances SMAD1 signaling, and suppresses age-related bone loss in male mice. J Cell Physiol 2023; 238: 566-581.
[31] Su H, Liang L, Wang J, Yuan X and Zhao B. ZFP36, an RNA-binding protein promotes hBMSCs osteogenic differentiation via binding with JUN. J Orthop Surg Res 2024; 19: 758.
[32] Zhang Z, Guo M, Li Y, Shen M, Kong D, Shao J, Ding H, Tan S, Chen A, Zhang F and Zheng S. RNA-binding protein ZFP36/TTP protects against ferroptosis by regulating autophagy signaling pathway in hepatic stellate cells. Autophagy 2020; 16: 1482-1505.
[33] Liu J, Song X, Kuang F, Zhang Q, Xie Y, Kang R, Kroemer G and Tang D. NUPR1 is a critical repressor of ferroptosis. Nat Commun 2021; 12: 647.
[34] Chen X, Yao Y, Gong G, He T, Ma C and Yu J. The potential role of AhR/NR4A1 in androgen-dependent prostate cancer: focus on TCDD-induced ferroptosis. Biochem Cell Biol 2025; 103: 1-11.
[35] Deng Y, Lu L, Zhu D, Zhang H, Fu Y, Tan Y, Tan X, Guo M, Zhang Y, Yang H, Yang B, Liu T and Chen Y. MafG/MYH9-LCN2 axis promotes liver fibrosis through inhibiting ferroptosis of hepatic stellate cells. Cell Death Differ 2024; 31: 1127-1139.
[36] Zhang W, Gao R, Rong X, Zhu S, Cui Y, Liu H and Li M. Immunoporosis: role of immune system in the pathophysiology of different types of osteoporosis. Front Endocrinol (Lausanne) 2022; 13: 965258.
[37] Zhou Y, Deng Y, Liu Z, Yin M, Hou M, Zhao Z, Zhou X and Yin L. Cytokine-scavenging nanodecoys reconstruct osteoclast/osteoblast balance toward the treatment of postmenopausal osteoporosis. Sci Adv 2021; 7: eabl6432.
[38] Liu J, Wang B, Chen H, Yu X, Cao X and Zhang H. Osteoclast-derived exosomes influence osteoblast differentiation in osteoporosis progression via the lncRNA AW011738/miR-24-2-5p/TREM1 axis. Biomed Pharmacother 2024; 178: 117231.
[39] Wang Q, Shen X, Chen Y, Chen J and Li Y. Osteoblasts-derived exosomes regulate osteoclast differentiation through miR-503-3p/Hpse axis. Acta Histochem 2021; 123: 151790.
[40] Gu C, Chen P, Tian H, Yang Y, Huang Z, Yan H, Tang C, Xiang J, Shangguan L, Pan K, Chen P, Huang Y, Liu Z, Tang R, Fan S and Lin X. Targeting initial tumour-osteoclast spatiotemporal interaction to prevent bone metastasis. Nat Nanotechnol 2024; 19: 1044-1054.
[41] Fischer V and Haffner-Luntzer M. Interaction between bone and immune cells: Implications for postmenopausal osteoporosis. Semin Cell Dev Biol 2022; 123: 14-21.
[42] Saxena Y, Routh S and Mukhopadhaya A. Immunoporosis: role of innate immune cells in osteoporosis. Front Immunol 2021; 12: 687037.
[43] Zhang P, Feng Q, Chen W and Bai X. Catalpol antagonizes LPS-mediated inflammation and promotes osteoblast differentiation through

the miR-124-3p/DNMT3b/TRAF6 axis. Acta Histochem 2024; 126: 152118.
[44] Peek CT, Ford CA, Eichelberger KR, Jacobse J, Torres TP, Maseda D, Latour YL, Piazuelo MB, Johnson JR, Byndloss MX, Wilson KT, Rathmell JC, Goettel JA and Cassat JE. Intestinal inflammation promotes MDL-1(+) osteoclast precursor expansion to trigger osteoclastogenesis and bone loss. Cell Mol Gastroenterol Hepatol 2022; 14: 731-750.
[45] Liang D, Minikes AM and Jiang X. Ferroptosis at the intersection of lipid metabolism and cellular signaling. Mol Cell 2022; 82: 2215-2227.
[46] Liu P, Wang W, Li Z, Li Y, Yu X, Tu J and Zhang Z. Ferroptosis: a new regulatory mechanism in osteoporosis. Oxid Med Cell Longev 2022; 2022: 2634431.
[47] Jing Z, Li Y, Zhang H, Chen T, Yu J, Xu X, Zou Y, Wang X, Xiang K, Gong X, He P, Fu Y, Ren M, Ji P and Yang S. Tobacco toxins induce osteoporosis through ferroptosis. Redox Biol 2023; 67: 102922.
[48] Jiang Z, Qi G, He X, Yu Y, Cao Y, Zhang C, Zou W and Yuan H. Ferroptosis in osteocytes as a target for protection against postmenopausal osteoporosis. Adv Sci (Weinh) 2024; 11: e2307388.
[49] Huo N, Xu G, Zhou H, Liu Y, Li S, Yang X, Liu J, Wang W, Yang N and Zhou N. Nanovesicles synergistically regulate ferroptosis characteristic macrophage-induced angiogenesis via ferritin heavy Chain 1/glutathione peroxidase 4 pathway to promote peripheral nerve regeneration. ACS Appl Mater Interfaces 2025; 17: 55876-55894.
[50] Zheng N, Li F, Huang Q, Huang X and Maj T. Macrophages and macrophage extracellular vesicles confer cancer ferroptosis resistance via PRDX6-mediated mitophagy inhibition. Redox Biol 2025; 86: 103826.

Table S1. Primer sequences used in the RT-qPCR analysis

Primers	Sequences
18S-F	CTGGATACCGCAGCTAGGAA
18S-R	GAATTTCACCTCTAGCGGCG
Nr4a1-F	CTTCGGCGTCCTTCAAGTTTG
Nr4a1-R	GGCTGGAAGTTGGGTGTAGA
Lcn2-F	AGCTGTCCCCTGAACTGAAG
Lcn2-R	TGATGTTGTCGTCCTTGAGG
Nupr1-F	GGGGAGGTCGGAAAGGTC
Nupr1-R	TGGAACTTGGTCAGCAGCT
Zfp36-F	CCGAATCCCTCGGAGGACTT
Zfp36-R	GAGCCAAAGGTGCAAAACCA